Mesomorphic Complexes of Poly(amidoamine) Dendrimer with DNA

Yi-Chun Liu,[†,‡] Hsin-Lung Chen,[*,†] Chun-Jen Su,[†] Hsien-Kuang Lin,[‡] Wen-Liang Liu,[‡] and U-Ser Jeng[§]

Department of Chemical Engineering, National Tsing Hua University, Hsin-Chu 30013, Taiwan, R.O.C., Materials Research Laboratories, Industrial Technology Research Institute, Chutung, Hsin-Chu, Taiwan, R.O.C., and National Synchrotron Radiation Research Center, Hsin-Chu 300, Taiwan R.O.C.

Received June 26, 2005; Revised Manuscript Received September 12, 2005

ABSTRACT: The self-assembly behavior of the complexes of DNA with fully surface-protonated poly(amidoamine) (PAMAM) dendrimer of generation four has been studied as a function of the overall complex composition. The complex composition (x) was expressed by the molar ratio of the positively charged ammonium groups in the dendrimer to the DNA base pairs. The complexation was found to result in DNA condensation through which the dendrimer-bound DNA chains aggregated significantly to form ordered structures. A condensed nematic phase in which the locally oriented DNA chains did not exhibit coherent positional order formed at $x = 2$. Although the numbers of positive and negative charges were identical at this composition, the charge matching was frustrated by the DNA−DNA repulsion which limited the number of DNA chains surrounding each dendrimer molecule. Therefore, the nematic mesophase was built up by the irregularly packed square columnar cells (with each dendrimer molecule surrounded by four DNA chains in each cell), yielding defective DNA networks with the average interhelical distance of 4.2 nm. A significant fraction of the phosphate groups on the DNA chains in the network remained unbound to the dendrimer due to limited supply of dendrimer molecules. The condensed DNA structure transformed into a long-range ordered square columnar phase with the interhelical distance of 4.25 nm at $x = 4.0$. Here the number of dendrimers became abundant enough to maximize the charge matching for the DNA chains, and the interconnection of the square columnar unit cells led to a long-range ordered lattice.

Introduction

Starburst dendrimers constitute a special class of hyperbranched macromolecule composed of layers of monomer units irradiating from a central core. Each complete grafting cycle is called a "generation" (denoted by Gn with n being the generation number). The global conformation of dendrimers resembles that of star polymer at low generations (< G4). Increasing the generation number increases the compactness of the dendrimer molecules and hence transforms the conformational characteristic to soft sphere at intermediate generations (∼ G4 to G8) and to hard sphere at high generations (> G8).[1]

Significant attention has been directed to the applications of dendrimers in biomedical and biochemical fields due to their biocompatibility and similarity with biological macromolecules such as globular proteins, antibodies, and histones in terms of their internal structure and size.[1−3] Dendrimers also bear the ability to bind with different biomolecules after proper functionalization. In particular, positively charged dendrimers can form electrostatic complexes with polyanionic DNA. In the presence of excess dendrimer, the DNA−dendrimer complex may carry an overall positive charge that favors its attachment to anionic animal cells; therefore, nonviral gene delivery for gene therapy has been considered as a promising application for this type of material.[4−8]

Since the supramolecular structure of the complexes may play a crucial role in their interactions with cells, various attempts have been made to reveal the self-assembled structures of DNA−dendrimer complexes using principally spectroscopic techniques.[9−11] It was believed that the DNA chains tended to coil around the cationic dendrimers despite large stiffness, leading to the beads-on-string configuration as that found in the DNA/histone complex.[12] Nevertheless, considering that cationic dendrimers are effectively macrocations, their interactions with DNA should induce DNA condensation (a well-known process driven by DNA interaction with multivalent cations) through which the molecularly dissolved wormlike DNA chains in aqueous solution aggregate and pack into ordered structures. We would then expect the complexation to generate condensed mesomorphic structures with ordering of DNA chains. The formation of these mesophases has recently been disclosed by Evans et al., who studied the complexes of DNA with fully protonated polypropylene(imine) (PPI) dendrimers of intermediate generation (i.e., G4 and G5).[13] The DNA chains in these complexes were found to organize into columnar mesophases with in-plane square or hexagonal symmetries depending upon the dendrimer generation number and dendrimer-to-DNA charge ratio. This finding greatly modified the commonly assumed beads-on-string model for the complexes.

Besides gene delivery, DNA−dendrimer complexes may also be considered as a nanostructural template in the light of the ordered DNA structures attained. Identifying the strategy for effectively engineering the self-assembly behavior of the complexes would become an even more important task for this application. In this article we study the self-assembly of the complex of DNA with poly(amidoamine) (PAMAM) G4 dendrimer. PAMAM dendrimer can be positively charged in acidic media

[†] National Tsing Hua University.
[‡] Industrial Technology Research Institute.
[§] National Synchrotron Radiation Research Center.

10.1021/ma0513620 CCC: $30.25
Published on Web 10/15/2005

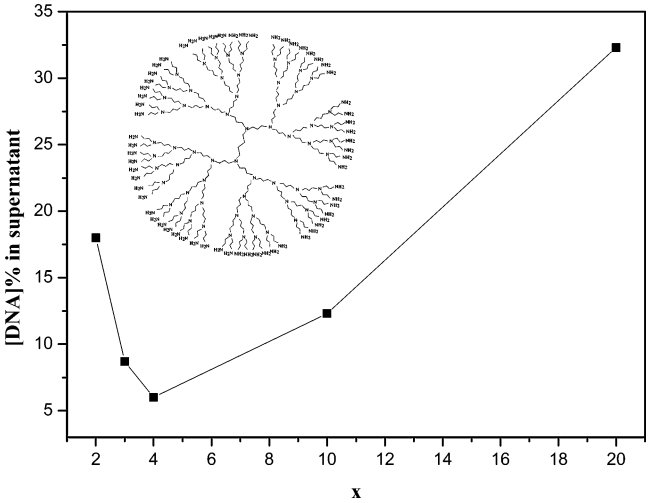

Figure 1. Percentage of DNA remained in the supernatant measured by the UV/vis spectroscopy as a function of x. The concentration was calculated by assuming the molar extinction coefficient of 6500 cm^2/mol for the DNA absorption peak centering at 260 nm. The curve displayed a minimum at $x \approx 4.0$, where nearly all DNA formed insoluble complexes with the dendrimer. The inset displays the chemical structure of PAMAM G4 dendrimer.

by proton transfer to the amine groups in the molecule. Here we center on the complex with fully surface-protonated dendrimer, with a detailed examination on the effect of the overall complex composition on the self-assembly behavior. It will be shown that the complex self-organized into two kinds of mesomorphic structures, namely, a nematic phase and a long-range ordered square columnar phase, depending upon the dendrimer-to-DNA molar ratio. The structures in terms of the spatial arrangements of DNA and dendrimers in these two types of mesophases will be analyzed in detail based principally on the small-angle X-ray scattering (SAXS) results. The secondary structure of DNA in the complexes will also be revealed from the scattering profiles in the wide angle region.

Experimental Section

Materials. Linear DNA type XIV from herring testes sodium salt (Na content 6.2%) was purchased from Sigma and used without further purification. Its molecular weight determined by gel electrophoresis was found to have a polydispersity value between 400 and 1000 base pairs (bp) with a center of distribution at ca. 700 bp.[14] PAMAM G4 dendrimer with the chemical structure shown in Figure 1 was acquired from Aldrich.

Complex Preparations. To complex with the polyanionic DNA, the amine groups in PAMAM dendrimer were first protonated by adding a prescribed amount of 0.2 M HCl solution. The 64 primary amine groups at the outer surface of the dendrimer tended to be protonated first because their basicity (p$K_a \cong 9.0$) was larger than that of the interior teriary amines (p$K_a \cong 5.8$).[15] Therefore, the fully surface-protonated PAMAM G4 dendrimer was prepared by adding into the 16 mg/mL aqueous solution a stoichiometric amount of HCl that was just sufficient to protonate all the $-NH_2$ groups at the dendrimer surface. The pH of the solution was 8.5, which situated closely to the reported range for the full surface protonation of PAMAM dendrimers.[15,16] The dendrimer solution was mixed with the aqueous solution containing prescribed amount of DNA to obtain the complex. The complexation was usually manifested by visually observable precipitation. The complex composition, x, was expressed by the molar ratio of the positively charged ammonium groups in the dendrimer to the DNA base pairs.

UV/Vis Measurements. UV absorption spectra were recorded with a Perkin-Elmer Lamda 900 spectrophotometer to measure the concentration of DNA remained in the supernatant upon complexation, assuming the molar extinction coefficient of 6500 cm^2/mol for the DNA absorption peak centering at 260 nm.[17] Prior to the measurement, the separation between the supernatant and the precipitate was facilitated by centrifugation at a speed of 3200 rpm for 10 min. Quartz cells with an optical path of 1 cm were used for the measurements.

Small-Angle X-ray Scattering (SAXS) Measurements. The self-assembled structures of the complexes in the fully hydrated state were probed SAXS at room temperature (ca. 27 °C). The aqueous suspensions of the complexes were directly introduced into the sample cell comprising of two Kapton windows. SAXS measurements were performed using a Bruker NanoSTAR SAXS instrument, which consisted of a Kristalloflex K760 1.5 kW X-ray generator (operated at 40 kV and 35 mA), cross-coupled Göbel mirrors for Cu Kα radiation (λ = 1.54 Å) resulting in a parallel beam of about 0.05 mm^2 in cross section at the sample position, and a Siemens multiwire-type area detector with 1024 × 1024 resolution mode. All data were corrected by the empty beam scattering and the sensitivity of each pixel of the area detector. The area scattering pattern has been circularly averaged to increase the efficiency of data collection. The intensity profile was output as the plot of the scattering intensity (I) vs the scattering vector, $q = 4\pi/\lambda \sin(\theta/2)$ (θ = scattering angle). The SAXS profiles reported here have also been corrected for thermal diffuse scattering (TDS). TDS was considered a positive deviation from Porod's law and may be associated with thermal motion, local disorder, or onset of wide-angle scattering region.[18] The intensity level of TDS was assumed to be a constant, and its magnitude was determined from the slope of the Iq^4 vs q^4 plot.

Results and Discussion

Similar to most polyelectrolyte complexes, the complexation of DNA with cationic dendrimers usually resulted in visually observable precipitation. The percentage of DNA remaining in the supernatant measured by the UV/vis spectroscopy was plotted as a function of x in Figure 1. A concave curve with a minimum located at $x \approx 4.0$ was observed. At $x < 4$ increasing x or the amount of dendrimer in the system demanded more DNA for charge neutralization; thus, the amount of DNA remained in the supernatant decreased accordingly. Nearly all DNA formed insoluble complexes with the dendrimers at $x = 4.0$; namely, the isoelectric point should locate at $x = 4.0$. Above this isoelectric point where the dendrimer was in significant excess of DNA in terms of ionic charge, the concentration of DNA in the supernatant was found to increase with increasing x. We proposed that the amount of dendrimers bound to DNA here was actually more than that necessary to neutralize the charges on DNA. In this case, overcharged complexes were formed by the adsorption of additional dendrimers onto the outer surface of the primary complexes having attained the optimum charge matching in the interior.[19,20] This adsorption was driven by the entropic gain from the counterion release.[21,22] More specifically, when a highly charged dendrimer adsorbed electrostatically onto the primary complex, a certain number of the originally condensed Cl^- counterions on the dendrimers were released as long as the net charge density of the complexes remained sufficiently low. It should be noted that a charge-neutral complex of macroions with no counterions cannot be in electrochemical equilibrium with free macroions in solutions that contained counterions.[23] The size of the aggregates of the overcharged complexes was limited by their mutual repulsion. These small complex aggregates remained well dispersed in the supernatant,

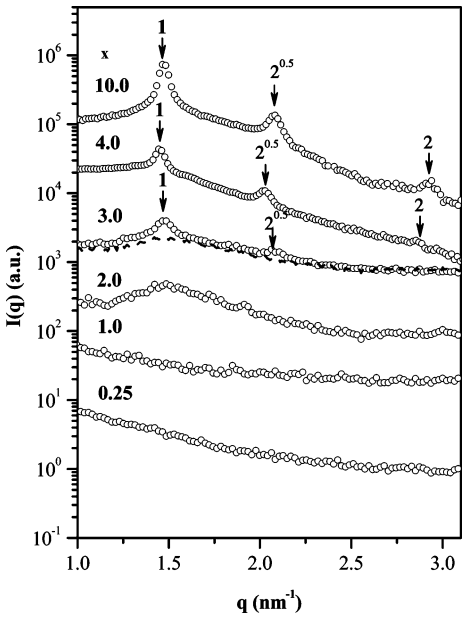

Figure 2. Room temperature SAXS profiles of the DNA–PAMAM G4 dendrimer complexes with different compositions. Monotonically decayed scattering curves were observed at $x < 2.0$, indicating that the DNA chains in the complexes were loosely packed without a rather well-defined interhelical distance. A broad DNA–DNA correlation peak corresponding to the formation of a condensed nematic phase was observed at $x = 2.0$. Multiple diffraction peaks with the position ratio of $1:2^{1/2}:4^{1/2}$ were visible at $x = 4.0$ and 10.0, signaling the formation of a long-range ordered square columnar phase. The nematic phase was found to coexist with a minor fraction of the square phase at $x = 3.0$.

leading to a higher DNA concentration in the supernatant at larger x.

The self-assembled structures of the complexes were probed by SAXS. The SAXS profiles of the complex precipitates were collected except at $x < 2.0$ where the (undercharged) complexes remained well dispersed in water without obvious precipitation. In this case, the SAXS profiles of the aqueous dispersions were obtained. Figure 2 displays the room temperature SAXS profiles of the complexes with different compositions. The complexes consisted of DNA, dendrimer, and trapped water, whose electron density was 0.885, 0.664, and 0.550 mol e/cm^3, respectively. Since the electron density of DNA was much larger than the other two species, it was reasonable to assume that the observed SAXS pattern was dominated by DNA, namely, the pattern related primarily to the spatial correlation of the DNA chains.

Three types of scattering profiles were distinguished in Figure 2. At $x < 2.0$, the complex displayed a monotonically decayed curve, signaling that the DNA chains in the complexes were loosely packed without a rather well-defined interhelical distance. In this case, the birefringent texture characteristic of mesomorphic phases was not observed under polarized optical microscopy (POM).

A broad DNA–DNA correlation peak corresponding to the interhelical distance ($d_{DNA} = 2\pi/q_m$ with q_m being the peak position) of 4.2 nm became visible when x increased to 2.0. The corresponding POM micrograph in Figure 3 revealed optically birefringent pattern, indicating that the DNA chains in the complex were orientationally ordered. The packing of these chains, however, lacked long-range positional order as the

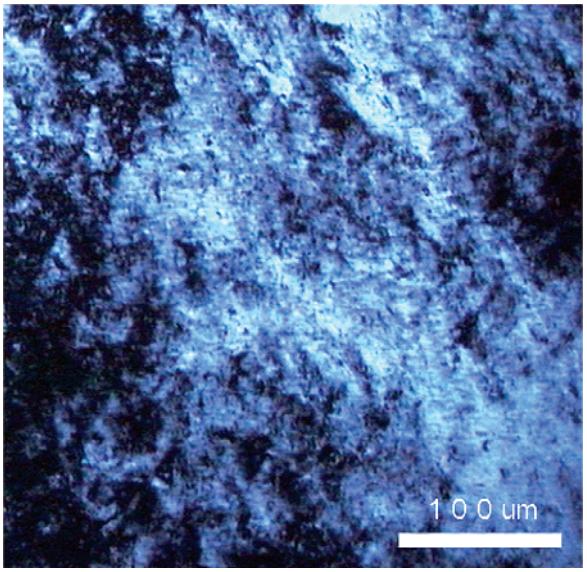

Figure 3. Polarized optical micrograph of the complex with $x = 2.0$, showing the presence of optically birefringent pattern characteristic of mesomorphic structures.

corresponding DNA–DNA correlation peak was broad. We hence designated the mesomorphic structure as a nematic phase. The stiff DNA chains in the nematic phase did not exhibit coherent positional order, but they tended to align toward a local director and consequently gave rise to anisotropic optical properties.

The complex exhibited another distinct scattering pattern at $x = 4.0$. Here the SAXS profile was characterized by a primary peak located at 1.5 nm^{-1} along with a weaker peak at 2.1 nm^{-1}. The ratio of the positions of these peaks was $1:2^{1/2}$, which corresponded closely to the lattice scattering from a 2-D square columnar phase with the lattice constant (i.e., the nearest interhelical distance) of 4.25 nm.[24] Significantly, the complex with $x = 10.0$ exhibited sharper diffraction peaks, and the third-order peak at 2.94 nm^{-1} became visible. The relative positions of the three peaks followed the ratio of $1:2^{1/2}:4^{1/2}$, which was again assignable to a square columnar phase. The nematic phase was found to coexist with a minor fraction of the square phase at $x = 3.0$, as the two square lattice peaks were found to superpose on a broad nematic peak (the dashed line). The interhelical distance in the square lattice remained virtually constant with respect to the change of x at least up to $x = 10.0$. This was different from that found for the complexes of DNA with fully protonated PPI G5 dendrimer, where an abrupt rise of d_{DNA} occurred near the isoelectric point.[13] It should be noted that the composition ($x = 4.0$) at which the square phase became the predominant structure corresponded well to the isoelectric point at which nearly all the DNA formed insoluble complex with the dendrimer as revealed in Figure 1. Consequently, the complex composition in the square columnar phase was approximately given by $x \approx 4.0$.

On basis of the SAXS results, DNA complex with fully surface-protonated PAMAM G4 dendrimer was found to undergo structural transitions from a noncondensed phase ($x < 2.0$) to a condensed nematic phase ($2.0 \le x < 4.0$) and finally to a long-range ordered square columnar phase ($x \ge 4.0$) with increasing x. Our result corroborated the study by Evans et al.[13] showing that the DNA–dendrimer complexes exhibited mesomorphic structures characterized by the positional and orienta-

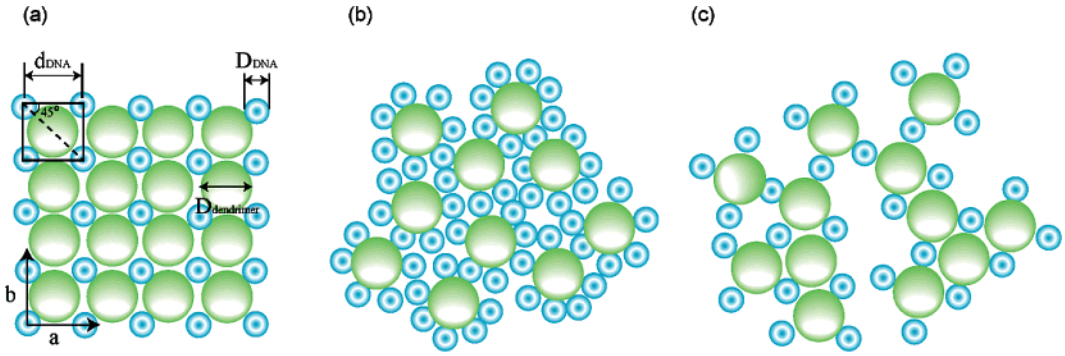

Figure 4. Schematic illustrations of the packings of DNA and dendrimers in the following mesophases from the top view: (a) square columnar phase with $d_{DNA}{}^{S} = 2^{-1/2}(D_{dendrimer} + D_{DNA})$, (b) a nematic phase with the dendrimer molecules surrounded by the maximum number of DNA chains to maximize the charge matching for DNA; (c) a nematic phase contained defective DNA networks built up by irregularly packed square columnar cells. The diameter of the cross section of DNA and that of the dendrimer were drawn according to their actual relative size, namely, the diameter of DNA, $D_{DNA} = 2.0$ nm and $D_{dendrimer} = 4.0$ nm $= 2D_{DNA}$.

tional order of DNA. The structural model was in clear distinction from the beads-on-string model deduced from the spectroscopic studies.[9−11] The contradiction may stem from the largely different concentrations of the DNA and the dendrimer solutions used for preparing the complexes, where the DNA concentrations (ca. 20−30 μg/mL) adopted in the previous studies were much lower than that (5−80 mg/mL) used here. In the dilute concentration regime where the DNA chains did not overlap, the probability of the primary complexes to aggregate to form mesomorphic structure was accordingly very low; in this case, the tendency to maximize the charge matching might drive the DNA chains to wrap around the dendrimer molecules and thereby yielded the beads-on-string configuration.

We now analyze the structures at different regimes in detail. At $x < 2.0$ where DNA was in excess of dendrimer in terms of ionic charge, undercharged complexes were formed by the adsorption of additional DNA onto the outer surface of the primary complexes due to the same reasoning proposed for the formation of the overcharged complexes. These small complex aggregates remained well dispersed in water, and the DNA chains within them were loosely packed without a well-defined interhelical distance.

A condensed nematic phase was formed when x increased to 2.0 where the numbers of positive and negative charges became identical. In this case, formation of a long-range ordered square lattice was implausible due to ineffective charge matching for the DNA chains under a limited supply of dendrimer. Figure 4a displays the top view of the square lattice in which the dendrimer molecules were accommodated in the interstitial region between the DNA rods. Since the complex composition in the square phase was $x \approx 4.0$, only one-half of the DNA chains in the system with the overall composition of $x = 2.0$ could enter into the lattice (suppose all the dendrimers were incorporated into the lattice). In this case, 50% of the surface charges on dendrimer were not used for charge matching with (the other 50%) DNA chains and were hence wasted.

Because the supply of dendrimer was not abundant at $x = 2.0$, the system might seek a structure that efficiently used the positive charges on the dendrimers to attain the maximum charge matching for DNA. In this case, each dendrimer molecule was surrounded by the maximum number of DNA chains, giving rise to the nematic packing shown in Figure 4b. This model was however in conflict with the following two experimental observations. First, because of the crowding of DNA chains surrounding the dendrimers, the average d_{DNA} in the model should be smaller than that in the corresponding square columnar phase; however, the observed d_{DNA} (= 4.2 nm) in the nematic phase was nearly identical with that (= 4.25 nm) in the square phase. Furthermore, the tight packing of the DNA chains in the model should prescribe a higher volume fraction of DNA (ϕ_{DNA}) than that in the square phase. To test this argument, we calculated ϕ_{DNA} in both mesophases by means of the three-dimensional correlation function defined as follows:[18]

$$\gamma_3(r) = \frac{\int_0^\infty I(q) q^2 \sin(qr)/qr \, dq}{\int_0^\infty I(q) q^2 \, dq} \tag{1}$$

The Porod's law at large q prescribes $\gamma_3(r)$ to adopt the following form at small radial distance[18]

$$\gamma_3(r) = 1 - \frac{1}{l_P} \tag{2}$$

where l_P is the Porod length. According to eq 2, l_P can be determined from the slope of $\gamma_3(r)$ at small r, as demonstrated in Figure 5 which displays the $\gamma_3(r)$ of the complexes with $x = 2.0$ and 10.0. The Porod length is related to the volume-to-surface area ratio (V/S) of the DNA cylinders via

$$l_P = 4(1 - \phi_{DNA})\left(\frac{V}{S}\right) \tag{3}$$

V/S of the DNA cylinder is simply given by $V/S \approx D_{DNA}/4$ with D_{DNA} being the diameter of DNA. Equation 3 is hence rewritten as

$$l_P = D_{DNA}(1 - \phi_{DNA}) \tag{4}$$

It will be shown latter that the DNA duplecies in the complexes adopted B conformation; thus $D_{DNA} = 2.0$ nm.[25] ϕ_{DNA} can then be calculated from eq 4 once l_P is determined from $\gamma_3(r)$. The volume fractions of DNA thus obtained were 0.14 and 0.19 for the nematic phase at $x = 2$ and the square phase at $x = 10$, respectively. The value of 0.19 for the square phase closely agreed with the value of 0.17 deduced directly from d_{DNA} via $\phi_{DNA} = \pi D_{DNA}{}^2/4 d_{DNA}{}^2$. Consequently, the actual volume fraction of DNA in the nematic phase was *lower* than

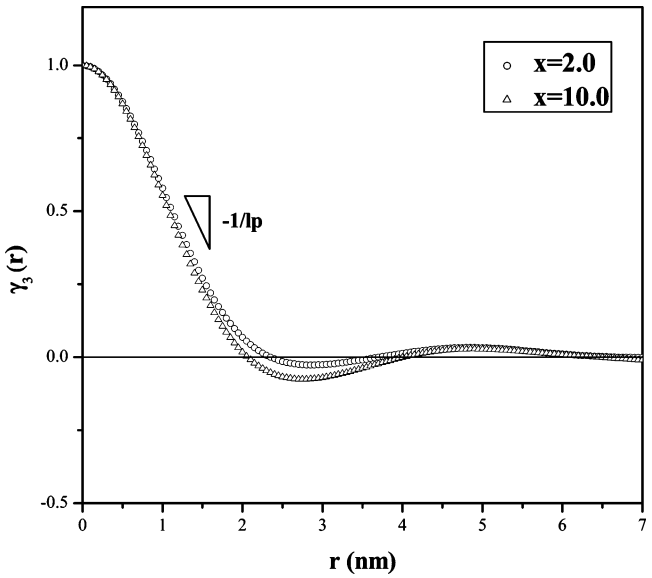

Figure 5. Three-dimensional correlation functions of the complexes with $x = 2.0$ and 10.0. The Porod length, l_P, was determined from the slope of $\gamma_3(r)$ at small r.

that in the square phase as more water was incorporated into the former.

The structure model for the nematic phase in Figure 4b was thus replaced by the one shown in Figure 4c that accommodated the two conditions, namely, $d_{DNA}{}^{N} \approx d_{DNA}{}^{S}$ and $\phi_{DNA}{}^{N} < \phi_{DNA}{}^{S}$ (where the superscripts "N" and "S" denote nenamtic and square phase, respectively). The new model postulated that the nematic phase was built up by the square columnar cells, but in contrast to those in the square columnar phase, these cells packed irregularly to form defective DNA networks. In this case, the interhelical distance in the defective DNA network was dominated by that in the square columnar cell, which was given by $d_{DNA} = 2^{-1/2}(D_{dendrimer} + D_{DNA}) = 4.25$ nm ($D_{dendrimer} = 4.0$ nm).[26] This value agreed well with the d_{DNA} deduced from the SAXS peak positions for the nematic and square phases. It appeared that the repulsion between the DNA chains surrounding the dendrimer molecules was strong, such that the free energy reduction by charge matching was unable to compensate the energetic penalty by having the maximum number of DNA chains to surround the dendrimers. The defective networks in the nematic phase contained more DNA chains (relative to the number of dendrimer molecules) than the perfect network in the square columnar phase; i.e., the corresponding dendrimer-to-DNA molar ratio was lower. In this case, a significant fraction of the phosphate groups on the DNA chains in the networks remained unbound to the dendrimer due to limited supply of dendrimer molecules. The adsorption of the poorly charge-matched DNA chains was however favored by the entropic gain from the counterion release. This entropic gain effectively compensated the loss in entropy of mixing of these DNA chains upon adsorption.

The DNA networks formed by the square columnar cells became less defective at larger x because the number of unbound phosphate groups was decreased by supplying more dendrimers for the charge matching. At $x = 4.0$ a perfect DNA network with long-range ordered square packing was formed. According to Figure 4a, each dendrimer molecule located in the interstitial region of the square lattice was surrounded by $4 \times (1/4) = 1.0$ DNA chain. The dendrimer molecules may stack along the longitudinal direction (i.e., c-axis) according to the models shown in Figure 6a,b. The dendrimer molecules in Figure 6a behaved like hard spheres as they stacked closely along the c-axis. The corresponding center-to-center distance of the dendrimer molecules along the c-axis was hence $D_{cc} = D_{dendrimer}$. The number of base pairs covered by a dendrimer molecule on average was hence given by

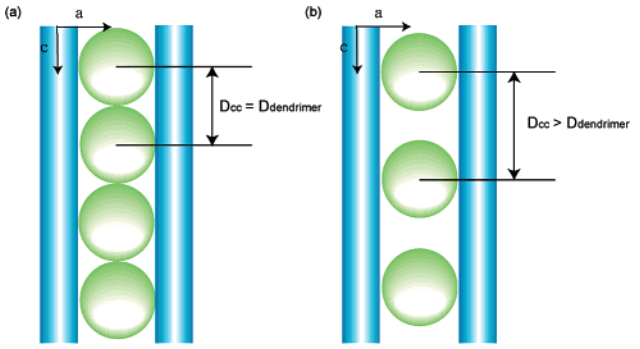

Figure 6. Schematic illustrations of the possible packings of dendrimer molecules along the DNA rod axis (i.e., c-axis). The dendrimer molecules in (a) behave like hard spheres as they stack closely along the c-axis. In this case the center-to-center distance between the dendrimer molecules is $D_{cc} = D_{dendrimer}$. Each dendrimer molecule in (b) is displaced by a distance from each other along the c-axis; thus $D_{cc} > D_{dendrimer}$.

$$n_{bp} = \frac{D_{cc}}{\text{3.4 nm per pitch in the DNA duplex}} \times (\text{10 base pairs per pitch}) = 11.8 \quad (5)$$

The composition of the complex forming this structure can then be calculated by

$$x = \frac{\text{64 ammonium groups in a dendrimer molecule}}{\text{11.8 base pairs}} = 5.4 \quad (6)$$

The calculated x was larger than the actual complex composition ($x = 4.0$) in the square columnar phase, meaning that the proposed model overestimated the number of dendrimer molecules encapsulated in the lattice.

Figure 6b proposed an alternative stacking model. Here we asserted that the close stacking of fully surface-protonated dendrimers in Figure 6a was energetically implausible because of strong electrostatic repulsion. To alleviate this repulsive interaction, each dendrimer molecule was displaced by a distance from each other along the c-axis, leaving water space between them. The center-to-center distance along the c-axis in this case was larger than $D_{dendrimer}$. If the complex composition in the square lattice was taken as $x = 4.0$, then D_{cc} deduced from eqs 5 and 6 was 5.44 nm.

The square columnar phase was the only long-range ordered structure observed for the present system. In a previous study of the DNA complexes with fully protonated PPI G4 dendrimer, Evans et al. have observed a hexagonal columnar phase at higher x.[13] They proposed that the lattice structure was governed by the competition between the long-range electrostatic cohesion that favored the square packing and the short-range electrostatic adhesion by counterion release that the favored the hexagonal structure. Here we would like to point

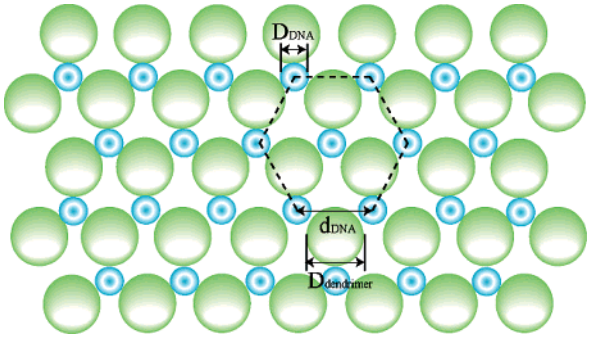

Figure 7. Schematic illustrations of how PAMAM G4 dendrimer molecules and DNA would arrange (from the top view) if the complex self-organized to form the hexagonal lattice. It can be seen that the hexagonal lattice contains more water space than the square lattice in Figure 4a.

out an additional factor that would favor the square packing over the hexagonal structure in the present complex system. Figure 7 schematically displays how PAMAM G4 dendrimer molecules and DNA would arrange (from the top view) if the complex self-organized to form the hexagonal lattice. It was not difficult to see from the model that the hexagonal lattice actually contained more water space than the square lattice in Figure 4a. Given that the interhelical distance in the hexagonal lattice was $d_{DNA}{}^{H} = 3^{1/2}/2(D_{dendrimer} + D_{DNA})$ and each dendrimer molecule was surrounded by $3 \times (1/3) = 1$ DNA chain; the volume fraction of water in the hexagonal lattice can be calculated by

$$\phi_w{}^{H} = 1 - \frac{\frac{\pi}{4}D_{DNA}{}^{2}L_{DNA} + \frac{4\pi}{3}\left(\frac{D_{dendrimer}}{2}\right)^{3}\left(\frac{L_{DNA}}{D_{cc}}\right)}{\frac{\sqrt{3}}{2}d_{DNA}{}^{H2}L_{DNA}}$$

$$= 1 - \frac{\frac{\pi}{4}D_{DNA}{}^{2} + \frac{\pi}{6}\left(\frac{D_{dendrimer}}{D_{cc}}\right)^{3}}{\frac{\sqrt{3}}{2}d_{DNA}{}^{H2}} \qquad (7)$$

where L_{DNA} is the length of the DNA chain. If the center-to-center distance of the dendrimer along the c-axis was taken as $D_{cc} = 5.44$ nm, then $\phi_w{}^{H}$ was found to be 0.60. In the case of square lattice, the volume fraction of water was given by

$$\phi_w{}^{S} = 1 - \frac{\frac{\pi}{4}D_{DNA}{}^{2} + \frac{\pi}{6}\left(\frac{D_{dendrimer}}{D_{cc}}\right)^{3}}{d_{DNA}{}^{S2}} \qquad (8)$$

Note that here $d_{DNA}{}^{S} = 2^{-1/2}(D_{dendrimer} + D_{DNA})$. $\phi_w{}^{S}$ calculated from eq 8 was 0.48, which was obviously lower than that in the hexagonal lattice. The high water content in the hexagonal lattice implied that a significant fraction of charges on the dendrimer and DNA were wasted. This can actually be visualized directly from the schematic illustration in Figure 7 as a large fraction of the periphery of the dendrimers failed to contact with DNA (and vice versa). Consequently, square packing was favored over hexagonal lattice due to more effective charge matching. It should be noted that the validity of this argument should depend on the size of the dendrimer. For dendrimers with low generation, each

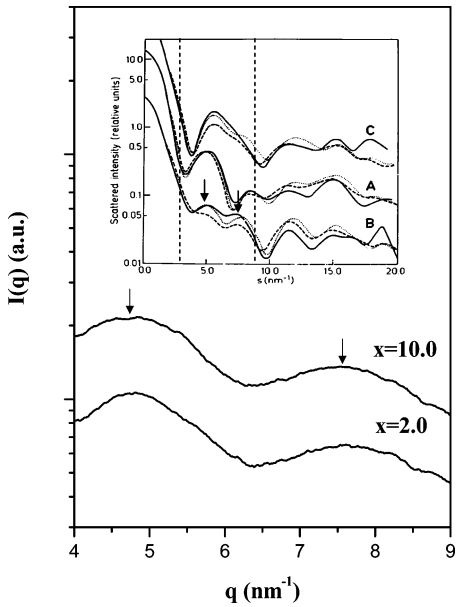

Figure 8. Scattering curves of the complexes with $x = 2.0$ and 10.0 in the q range from 4 to 9 nm^{-1}. Both compositions were found to exhibit two broad peaks situating at 4.9 and 7.4 nm^{-1}. The inset displays the scattering curves of the three conformational forms (A, B, and C) of DNA calculated by Müller.[26] The observed scattering patterns closely matched that of B-form DNA in the region enclosed by the dashed lines.

DNA chain may be surrounded by more dendrimer molecules, and then hexagonal lattice would lead to more compact packing (and hence more effective charge matching). Our ongoing study of the complex of DNA with PAMAM G2 dendrimers actually supports this view as the complex was found to display hexagonal columnar structure (see Supporting Information).

Finally, with the aid of the X-ray scattering in the high-q region, we would like to identify the secondary structure of the DNA in the mesomorphic complexes to reveal whether the electrostatic interaction with dendrimer could perturb the duplex conformation. The use of scattering intensity vs q plot to reveal the secondary structure of DNA has already been demonstrated two decades ago by Müller, who calculated the scattering patterns for DNA with A, B, and C conformation[27] (cf. inset of Figure 8). Therefore, the DNA conformation in the complexes can be disclosed conveniently by comparing the experimentally observed intensity profiles with the calculated ones in the appropriate q region. Figure 8 displays the scattering curves of the complexes with $x = 2.0$ and 10.0 in the q range from 4 to 9 nm^{-1} (9 nm^{-1} was about the maximum accessible q for our SAXS setup). Both compositions were found to exhibit two peaks situating at 4.9 and 7.4 nm^{-1}. The observed scattering patterns matched that of B-form DNA shown in the inset. The B conformation is the most common secondary structure of DNA in the fully hydrated state. Our X-ray scattering results indicated that the B conformation of DNA was not perturbed by the electrostatic binding with dendrimer. Furthermore, the fact that the DNA chains in both the nematic and the square phases adopted the B conformation attested that the supramolecular structure was independent of the DNA secondary structure. In this case, the formation of mesomorphic structures was prescribed by the geometric features of dendrimer and DNA at the coarse-grained level, where the former and the latter can be represented by sphere and rod (at the length scale smaller

than the persistent length of ca. 50 nm[28]), respectively, irrespective of the DNA duplex conformation.

Conclusions

The mesomorphic structures of the complexes of DNA with fully surface-protonated PAMAM G4 dendrimer have been studied by means of SAXS. Two types of mesomorphic structures characterized by different degrees of DNA ordering have been observed. At $2 \leq x < 4$ the complex exhibited a condensed nematic phase in which the positional order of the DNA chains was of short range. In this case, the tendency to attain the maximum charge matching for DNA was frustrated by the DNA−DNA repulsion as the free energy reduction by charge matching failed to compensate the energetic penalty by having the maximum number of DNA chains to surround the dendrimer molecules. As a result, defective DNA networks built up by the irregularly packed square columnar cells were formed under the limited supply of dendrimer. The DNA networks formed by the square columnar cells became less defective at larger x and perfect networks consisting of DNA chains packed into a long-range ordered square lattice were formed at $x = 4.0$. The square columnar phase was characterized by the interhelical distance of 4.25 nm and the center-to-center distance between the dendrimer molecules along the DNA rod axis of 5.44 nm. The square packing was favored over hexagonal lattice for the present system due to more effective charge matching. Finally, the X-ray scattering pattern in the high-q region revealed that the B conformation of DNA was not perturbed by the complexation with dendrimer in both the nematic and square phases.

Acknowledgment. This work was supported by the Industrial Technology Research Institute, Taiwan, under Grant A331XS9E00.

Supporting Information Available: Room temperature SAXS profiles of the complexes of DNA with fully surface protonated PAMAM G2 dendrimer with different charge ratios. This material is available free of charge via the Internet at http://pubs.acs.org.

References and Notes

(1) Prosa, T. J.; Bauer, B. J.; Amis, E. J. *Macromolecules* **2001**, *34*, 4897.
(2) Tomalia, D. A.; Hall, M.; Hedstrand, D. M. *J. Am. Chem. Soc.* **1987**, *109*, 1601.
(3) Bielinska, A. U.; Chen, C.; Johnson, J.; Baker, J. R., Jr. *Bioconjugate Chem.* **1999**, *10*, 843.
(4) Shchepinov, M. S.; Udalova, I. A.; Bridgman, A. J.; Southern, E. M. *Nucleic Acid Res.* **1997**, *25*, 4447.
(5) Bielinska, A. J. *Polym. Mater. Sci. Eng.* **1995**, *73*, 273.
(6) Boussif, O.; Lezoualc'h, F.; Zanta, M. A.; Mergny, M. D.; Scherman, D.; Demeneix, B.; Behr, J.-P. *Proc. Natl. Acad. Sci. U.S.A.* **1995**, *92*, 7297.
(7) Tang, M.; Redemann, C. T.; Szoka, F. C., Jr. *Bioconjugate Chem.* **1996**, *7*, 703.
(8) Haensler, J.; Szoka, F. C., Jr. *Bioconjugate Chem.* **1993**, *4*, 372.
(9) Ottaviani, M. F.; Sacchi, B.; Turro, N. J.; Chen, W.; Jockusch, S.; Tomalia, D. A. *Macromolecules* **1999**, *32*, 2275.
(10) Ottaviani, M. F.; Furini, F.; Casini, A.; Turro, N. J.; Jockusch, S.; Tomalia, D. A.; Messori, L. *Macromolecules* **2000**, *33*, 7842.
(11) Chen, W.; Turro, N. J.; Tomalia, D. A. *Langmuir* **2000**, *16*, 15.
(12) Stryer, L. *Biochemistry*; W.H. Freeman and Company: San Francisco, 1981.
(13) Evans, H. M.; Ahmad, A.; Ewert, K.; Pfohl, T.; Martin-Herranz, A.; Bruinsma, R. F.; Safinya, C. R. *Phys. Rev. Lett.* **2003**, *91*, 7, 075501-1.
(14) Dias, R.; Mel'nikov, S.; Lindman, B.; Miguel, M. G. *Langmuir* **2000**, *16*, 9577.
(15) Cakara, D.; Kleimann, J.; Borkovec, M. *Macromolecules* **2003**, *36,* 4201.
(16) Chen, W.; Tomalia, D. A.; Thomas, J. L. *Macromolecules* **2000**, *33*, 9169.
(17) Sambrook, J.; Fritsch, E. F.; Maniatis, T. *Molecular Cloning: A Laboratory Manual*; Cold Spring Harbor Laboratory Press: New York, 1989.
(18) Roe, R.-J. *Methods of X-ray and Neutron Scattering in Polymer Science*; Oxford University Press: New York, 2000.
(19) Tsuboi, A.; Izumi, T.; Hirata, M.; Xia, J.; Dubin, P. L.; Kokufuta, E. *Langmuir* **1996**, *12*, 6295.
(20) Takahashi, D.; Kubota, Y.; Kokai, K.; Izumi, T.; Hirata, M.; Kokufuta, E. *Langmuir* **2000**, *16*, 3133.
(21) Record, M. T., Jr.; Anderson, C. F.; Lohman, T. M. *Q. Rev. Biophys.* **1978**, *11*, 103.
(22) Park, S.Y.; Bruinsma, R. F.; Gelbart, W. M. *Europhys. Lett.* **1999**, *46*, 454.
(23) Bruinsma, R. *Eur. Phys. J. B* **1998**, *4*, 75.
(24) Knaapila, M.; Stepanyan, R.; Horsburgh, L. E.; Monkman, A. P.; Serimaa, R.; Ikkala, O.; Subbotin, A.; Torkkeli, M.; ten Brinke, G. *J. Phys. Chem. B* **2003**, *107*, 14199.
(25) Podgornik, R.; Rau, D. C.; Parsegian, V. A. *Macromolecules* **1989**, *22*, 1780.
(26) Tomalia, D. A.; Naylor, A. M.; Goddard III, W. A. *Angew. Chem., Int. Ed. Engl.* **1990**, *29*, 138.
(27) Müller, J. J. *J. Appl. Crystallogr.* **1983**, *16*, 74.
(28) Hagerman, P. J. *Annu. Rev. Biophys. Biophys. Chem.* **1988**, *17*, 265.

MA0513620